Broadband and Tunable High-Performance Microwave Absorption of an Ultralight and Highly Compressible Graphene Foam

Yi Zhang, Yi Huang,* Tengfei Zhang, Huicong Chang, Peishuang Xiao, Honghui Chen, Zhiyu Huang, and Yongsheng Chen

With the rapid arising of information technology, especially the explosive advance of novel multiband, broadband, or high-power electronic instruments, such as satellite communication, synthetic aperture radar, and ultra wide band radar, a high-performance microwave absorption (MA) material with a broadband MA ability is highly demanded to eliminate adverse electromagnetic waves effectively in healthcare, electronic safety, and national defense security.[1–3] In addition, the MA material enjoying the advantage of low density and thin thickness will be much favored in the fields of aerospace, aviation, automobile, and fast-growing new-generation miniaturized electronics.[3,4] Conventionally, separate solid particles, such as ferrites, metallic magnets, ceramics, and their hybrids are widely utilized as fillers into matrices to fabricate these MA materials. Despite good MA performance in some cases, their drawbacks, such as high density, poor stability, and large loading content, have severely hindered their practical applications.[5,6]

Recently, graphene materials have grabbed considerable attention for electromagnetic wave suppression due to their varieties of remarkable properties, including low density, high specific surface area, large aspect ratios, and versatile processing.[2,4,6–11] However, sole graphene material suffers from poor dispersion in the matrix,[10,11] interfacial impedance mismatching due to improper electrical conductivity,[2,7] and limited loss mechanism.[4,6] Therefore, incorporation of other lossy materials has been widely studied as the imperative solution to improve its MA performance.[2,6,7,10–12] However, to date, the absorption bandwidths of reflection loss (RL) less than −10 dB for all graphene-based MA composites ever reported have been only a few gigahertz, much narrower than those of traditional broadband microwave absorbents such as carbonyl iron.[2,4–7,10,11] Furthermore, important as it is for the practical application,[13] much less effort has been devoted to the convenient absorption regulation of an existing graphene-based MA material compared to unhandily changing either coating

Y. Zhang, Prof. Y. Huang, T. Zhang, H. Chang, P. Xiao,
H. Chen, Z. Huang, Prof. Y. Chen
Key Laboratory of Functional Polymer Materials,
Collaborative Innovation Center of Chemical Science
and Engineering (Tianjin)
Centre for Nanoscale Science and Technology,
Institute of Polymer Chemistry, College of Chemistry
Nankai University
Tianjin 300071, China
E-mail: yihuang@nankai.edu.cn

thickness or loading content. Lately, significant progress has been made toward investigating the synthesis of 3D interconnected graphene networks from 2D graphene sheets.[14–22] Using self-assembly method, very recently, we have synthesized a macroscopic 3D free-standing graphene foam (GF) characterized with air-similar densities, adjustable electrical conductivity, and ultrahigh compressibility,[23] which paves the way for the exploitation of graphene as a superlight, adjustable, and broadband high-performance MA material.

Herein, we demonstrate the broadband and tunable high-performance MA property of an ultralight and highly compressible GF. The GF exhibits a good MA performance in the measured frequency ranges of 2–18, 26.5–40, and 75–110 GHz (the total bandwidth of 64.5 GHz), which are occupied for many critical applications, including radar detections, satellite communications, and remote sensing.[24] Furthermore, the MA performance of the GF can be tuned very efficiently via a simple mechanical compression. Remarkably, the GF under 90% compressive strain achieves the absorption bandwidth (RL ≤ −10 dB) of 60.5 GHz, about 70% wider than that of the best available MA material in open literatures.[25] The individual 3D conductive network of the graphene sheets is thought to be the main reason behind the impressive MA ability of the GF.

The macroscopic GF for MA tests (Figure S1, Supporting Information) was prepared in a solvothermal process using a custom Teflon-lined autoclave, followed by thermal reduction and cutting treatments. The Raman spectrum (Figure S2, Supporting Information) and X-ray diffraction (XRD) pattern (Figure S3, Supporting Information) show that the GF is composed of reduced graphene oxide sheets with little long-range restacking. The cross-sectional SEM images (Figure S4, Supporting Information) indicate the 3D interconnected graphene network of the GF. The resultant GF has an ultralow bulk density of 1.4 mg cm^{-3}, over three orders of magnitude lower than most MA materials in open literature.[25–30] Considering the low intrinsic density of graphene sheets, the porosity more than 99% can be obtained, exceeding those of most foams used for microwave attenuation.[31–33]

The material's MA ability was evaluated based on the arch method developed by the U.S. Naval Research Laboratory, which is expressed as a curve of RL versus frequency.[34] The frequency bandwidth of RL ≤ −10 dB is generally considered as the qualified frequency bandwidth.[34,35] The broader the qualified frequency bandwidth is, the better performance the material presents. The MA performance of the best available MA materials reported before is listed in detail in Table S1, Supporting Information, for comparison, from which some
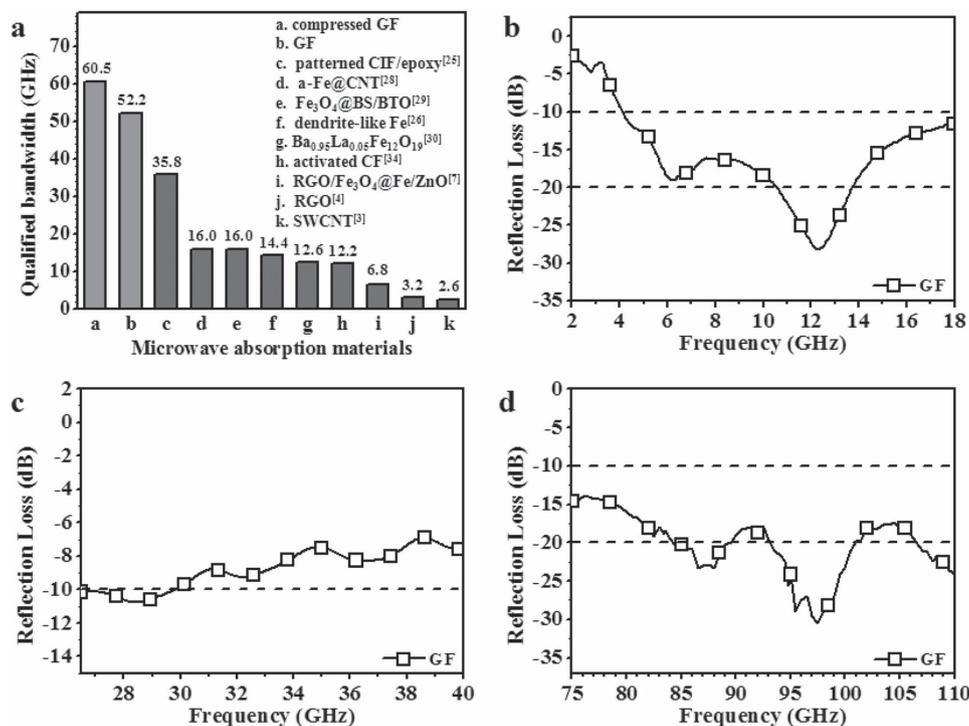
Figure 1. a) Direct comparison of the MA performance of the GFs (light gray columns (marked 60.5 and 52.2 GHz)) in this work with those of the representative materials (dark gray columns). The RL curves for the pristine GF are shown in b) 2–18; c) 26.5–40; and d) 75–110 GHz.

representative MA materials are chosen for a further direct comparison with the GFs in **Figure 1**a. In the whole frequency bands of 2–18, 26.5–40, and 75–110 GHz, the GF exhibits a very good MA performance (Figure 1b–d). Its qualified frequency bandwidth reaches 52.2 GHz, covering 80.9% of the entire measured bandwidth, which is much wider than those of most MA materials reported previously,[25,26,28–30,34] including all graphene-based composites.

As mentioned in our previous work, the additive-free GF could bear a high compressive strain over 90%.[23] It is thus essential to examine the effect of compression on the MA behavior of the GF in the whole frequency bands. For convenience, the GFs under different compressive strains of 30%, 60%, and 90% were marked as GF-30, GF-60, and GF-90, correspondingly. With the applied compressive strain increasing, the void space shrinks and the solid matrix grows denser as shown in **Figure 2**a–d. Notably, the walls randomly distributed originally stack obviously in parallel-aligned arrays perpendicular

to the compressing direction when the GF is highly compressed (Figure 2c,d). **Figure 3**a–c give the RL curves of the GFs under different compressive strains in 2–18, 26.5–40, and 75–110 GHz, respectively. It can be seen that the MA performance of the GF improves greatly with the applied compressive strains. When compressed to 10% of the original thickness, the GF demonstrates a substantial enhancement of the maximum RL value from −7.6 to −33.2 dB. Remarkably, GF-90, with a thin thickness of 1.0 mm, demonstrates the qualified frequency bandwidth as wide as 60.5 GHz, which covers 93.8% of the entire measured frequency bands, including the whole bands of X (8–12 GHz), Ku (12–18 GHz), Ka (26.5–40 GHz), W (75–110 GHz), and half of the C band (4–8 GHz).[36] Because light weight and thickness account for a considerable proportion in designing and evaluating microwave attenuation materials applied in aerospace, aviation, and ground vehicles,[37] here, we introduce a concept of the specific microwave absorption performance (integral of the RL curve divided by product of
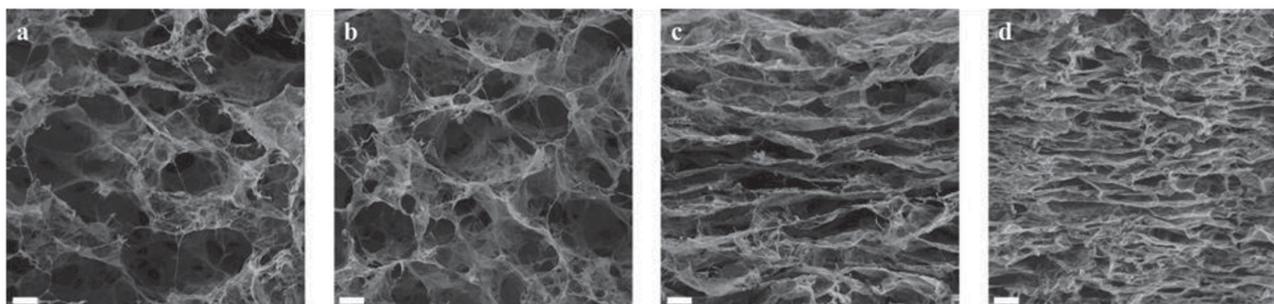

Figure 2. The cross-sectional SEM images of a) GF, b) GF-30, c) GF-60, and d) GF-90. The scale bar is 20 μm.
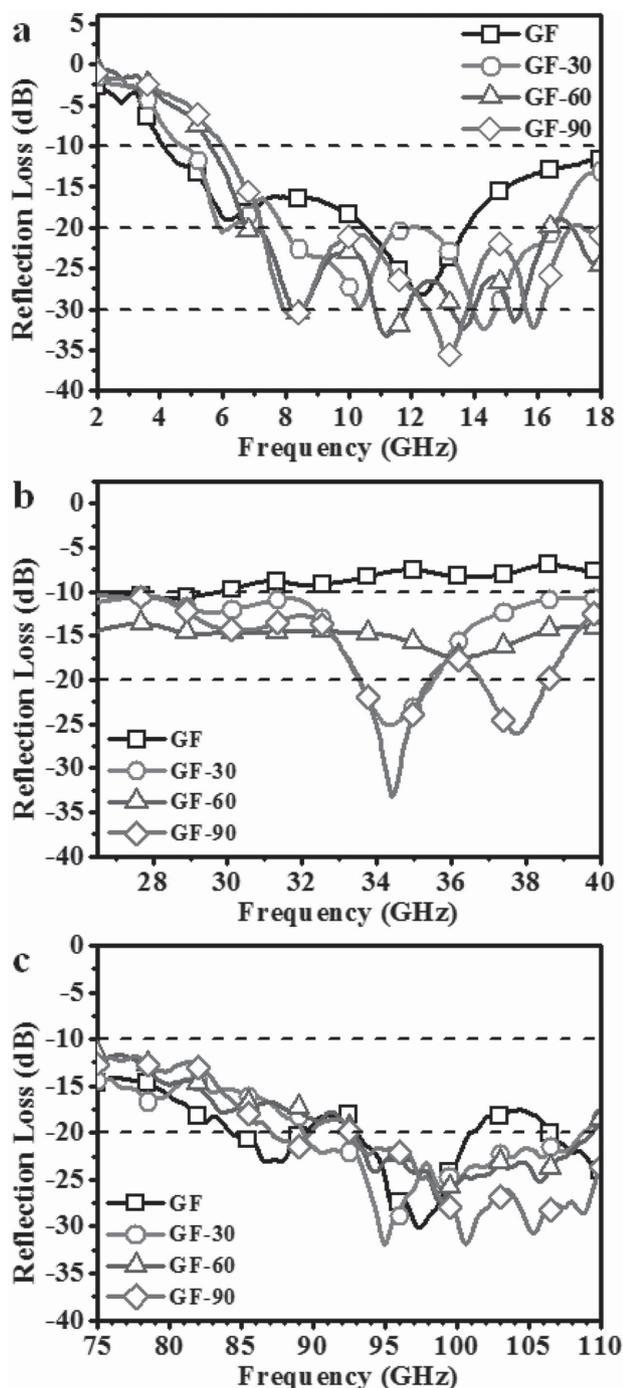
Figure 3. The RL curves for the GFs under different compressive strains are shown in a) 2–18; b) 26.5–40, and c) 75–110 GHz.

the density and the thickness; For more details, please see the Supporting Information) to evaluate the MA performance more comprehensively. The specific MA performance of the typical carbonyl iron-based MA material reaches ≈3.1 × 10^2 dB cm^2 g^{-1} in the measured frequency band of 2–18 GHz.[25] The α-Fe encapsulated within carbon nanotube/epoxy composite shows a higher specific MA performance of ≈2.0 × 10^3 dB cm^2 g^{-1} in the same frequency band.[28] Notably, the excellent MA

performance combined with the ultralow density (14 mg cm^{-3}) gives the GF a superior specific MA performance as high as 2.2 × 10^5 dB cm^2 g^{-1}, over two orders of magnitude higher than those of the best available MA materials reported before.

We also analyzed the MA mechanism of the GF. When electromagnetic radiation is incident on a material backed with a reflective metal (**Figure 4**a), the incident microwave power (P_{in}) is divided into two parts—the reflected microwave power (P_r) and the absorbed microwave power (P_a).[3] Therefore, a MA material would give an excellent performance only when the incident microwave penetrates the material deeply and then is absorbed and converts into heat by the absorbent as much as possible.[27]

When the incident microwave propagates at the interface between air and the MA material, undesirable reflection increases drastically due to the interfacial impedance gap.[2,10] The smaller real permittivity, according to the Weston's theorem, would result in less backscattered microwave for the dielectric carbon-based material.[13,38] The real permittivity of the GFs in 2–18 GHz is shown in Figure 4b. It can be found that owing to ultrahigh porosity over 99%, the uncompressed GF exhibits very low real permittivity which approximates that of single low-loss polymer such as poly(dimethyl siloxane)[10] and poly(ethylene oxide),[11] much lower than that of the conventional MA materials.[3,26,30] Furthermore, although the real permittivity of the compressed GF increases a lot with the rising compressive strain (Figure 4b), the same proportionate reduction in the thickness ensures penetrating of most incident microwave into the GF. Particularly, the cell wall of the GF is composed of only several entangled graphene sheets with a total thickness less than 5 nm (Figure S5, Supporting Information), much thinner than those of typical microwave attenuation foams.[32,33] This unique structure greatly shortens the impedance gap and weakens back reflection and scattering among struts and cell walls outside the GF, which contributes to the transmission of the incident microwave through the whole foam and thus boosts the GF absorption of radiation energy.

In most cases, the MA ability of the graphene is attributed to the polarization relaxation of defects or π-electron and interfacial polarization between graphene and other materials such as synergetic microwave absorbents and polymer matrices (Figure 4a).[2,4–7,10] However, compared to those of previous graphene-based MA composites, the higher dielectric loss tangent ($\tan \delta_e = \varepsilon''/\varepsilon'$) of the GF indicates that the individual 3D interconnected graphene network plays a key role in the substantially enhanced MA behavior (Figure 4c). The intricate reticulated structures consisting of entangled conductive graphene sheets spontaneously and intensely response to the broadband incident microwave as tremendous resistance–inductance–capacitance coupled circuits and time-varying electromagnetic fields-induced currents occur on cell walls and struts of the GF (Figure 4a).[39,40] Such long-range induced currents quickly attenuate in the resistive network and convert into thermal energy, leading to rapid decay of massive incident electromagnetic wave. Compared to the pristine one, the compressed GF shows an enhanced dielectric loss (Figure 4c), which is closely associated with the 3D structure transforming during compression. The void space shrinking
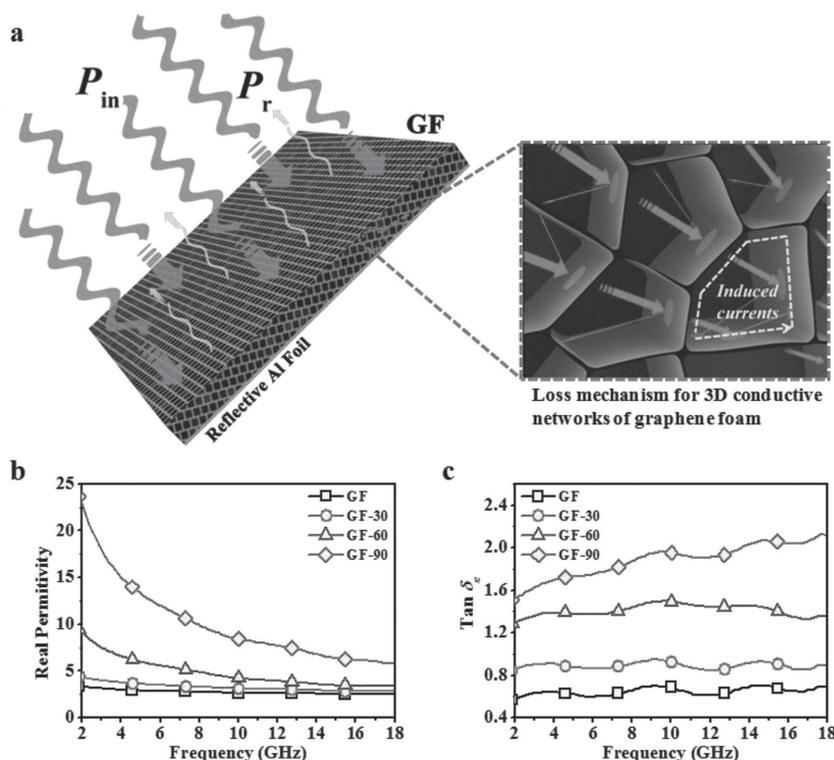
Figure 4. a) Schematic representation of the MA mechanism for the GF. b) Real parts of the complex permittivity of the GFs in the range 2–18 GHz. c) Dielectric loss tangent of the GFs in the range 2–18 GHz.

opens up the opportunity for the application of graphene as an ultralight and tunable high-performance broadband MA material in frontiers such as new-generation flexible privacy protection against electronic surveillance and stealthy combat units with high pay load.

Experimental Section

Synthesis of GF: The raw material, graphene oxide (GO), was prepared by oxidation of natural graphite powders using a modified Hummers method, as described elsewhere.[23] After differential centrifugation, the resultant GO ethanol solution (0.25 mg mL^{-1}) was solvothermally treated in a custom Teflon-lined autoclave (ϕ160 × 25 mm) at 180 °C for 12 h to form an ethanol-filled intermediate solid (ϕ120 × 10 mm). The gradient elution was then applied to replace the internal ethanol with water. After the solvent exchanging, the water-filled foam was freeze-dried to remove the remaining water inside. The resultant graphene oxide foam was annealed at 600 °C for 1 h in argon at ramp rate of 10 °C min^{-1} to obtain the GF.

Characterization: Based on the Arch method, the MA performance was evaluated in the range 2–18 GHz using an Agilent HP8757E scalar quantity network analyzer, in the range 26.5–40 GHz using an Agilent N5244A vector network analyzer and in the range 75–110 GHz using an Agilent N8257D vector network analyzer combined with a frequency multiplier, respectively. To keep reproducibility, four GFs cut into 90 × 90 × 10 mm were arranged in the closed cubic container with internal dimensions of 180 × 180 × 15 mm for measurements in the frequency band of 2–18 and 26.5–40 GHz. One GF cut into 60 × 60 × 10 mm was arranged in the closed cubic container with internal dimensions of 60 × 60 × 15 mm for measurement in the range 75–110 GHz. The containers with thin rigid mobile covers are made of polyvinyl chloride (PVC), which is nearly transparent to the incident microwave (Figure S7, Supporting Information). All GFs were backed with a highly conductive aluminum foil with the thickness of 30 μm to reflect all the incident microwave back to the receiving antenna. The GF under certain compression strain was achieved by fixing the mobile cover to the premarked position on the box.

The relative complex permittivity and permeability were measured in the frequency range of 2–18 GHz using an Agilent HP8722ES vector network analyzer. Paraffin was used as the supporting matrix due to its minor complex electromagnetic parameters approximating those of air. The toroidal test sample (3 mm i.d., 7 mm o.d., and 2 mm thickness) was fabricated by vacuum-impregnating the GF with paraffin. The incident microwave direction was perpendicular to the test sample.

Supporting Information

Supporting Information is available from the Wiley Online Library or from the author.

leads to more physical contacts between conductive graphene sheets, therefore increasing the resonance circuit density, which is consistent with the rising electrical conductivity of the GF (Figure S6, Supporting Information). What's more, the evolving horizontal-oriented entangled graphene alignment not only allows graphene sheets with high aspect ratio to form more horizontal conductive systems, but also enlarges effective absorption regions perpendicular to the electromagnetic wave incident direction, which has also been discussed in the electromagnetic shielding of graphene-based materials.[41,42]

In conclusion, we have demonstrated the broadband and tunable high-performance MA property of an ultralight and highly compressible GF. Compared with previous graphene-based MA composites, the GF delivers a substantially enhanced MA performance with the qualified frequency bandwidth of 50.5 GHz, covering 80.9% of the overall bandwidth (64.5 GHz). Furthermore, the MA performance can be effectively tuned simply by physically compressing it. Particularly, the GF under 90% compressive strain (1.0 mm thickness) obtains the qualified bandwidth of 60.5 GHz, covering 93.8% of the total frequency bands, about 70% wider than that of the best available MA material in open literatures. The excellent MA performance combined with ultralow density of 14 mg cm^{-3} gives the GF under 90% compressive strain an extraordinary specific MA performance as high as 2.2×10^5 dB cm^2 g^{-1}, which is over two orders of magnitude higher than those of the best available MA materials reported before. The 3D conductive network of the GF serves as the key that really

Materials
Views

www.MaterialsViews.com

ADVANCED
MATERIALS

www.advmat.de

COMMUNICATION

[1] T. Liu, Y. Pang, M. Zhu, S. Kobayashi, *Nanoscale* **2014**, *6*, 2447.
[2] L. Wang, Y. Huang, X. Sun, H. Huang, P. Liu, M. Zong, Y. Wang, *Nanoscale* **2014**, *6*, 3157.
[3] Z. Liu, G. Bai, Y. Huang, F. Li, Y. Ma, T. Guo, X. He, X. Lin, H. Gao, Y. Chen, *J. Phys. Chem. C* **2007**, *111*, 13696.
[4] V. K. Singh, A. Shukla, M. K. Patra, L. Saini, R. K. Jani, S. R. Vadera, N. Kumar, *Carbon* **2012**, *50*, 2202.
[5] D. Sun, Q. Zou, Y. Wang, W. Jiang, F. Li, *Nanoscale* **2014**, *6*, 6557.
[6] X. J. Zhang, G. S. Wang, W. Q. Cao, Y. Z. Wei, J. F. Liang, L. Guo, M. S. Cao, *ACS Appl. Mater. Interfaces* **2014**, *6*, 7471.
[7] Y. L. Ren, H. Y. Wu, M. M. Lu, Y. J. Chen, C. L. Zhu, P. Gao, M. S. Cao, C. Y. Li, Q. Y. Ouyang, *ACS Appl. Mater. Interfaces* **2012**, *4*, 6436.
[8] J. Liang, Y. Wang, Y. Huang, Y. Ma, Z. Liu, J. Cai, C. Zhang, H. Gao, Y. Chen, *Carbon* **2009**, *47*, 922.
[9] B. Wen, M. Cao, M. Lu, W. Cao, H. Shi, J. Liu, X. Wang, H. Jin, X. Fang, W. Wang, J. Yuan, *Adv. Mater.* **2014**, *26*, 3484.
[10] L. Kong, X. Yin, X. Yuan, Y. Zhang, X. Liu, L. Cheng, L. Zhang, *Carbon* **2014**, *73*, 185.
[11] X. Bai, Y. Zhai, Y. Zhang, *J. Phys. Chem. C* **2011**, *115*, 11673.
[12] Y. Ren, C. Zhu, S. Zhang, C. Li, Y. Chen, P. Gao, P. Yang, Q. Ouyang, *Nanoscale* **2013**, *5*, 12296.
[13] H. Sun, R. Che, X. You, Y. Jiang, Z. Yang, J. Deng, L. Qiu, H. Peng, *Adv. Mater.* **2014**, *26*, 8120.
[14] Z. Chen, W. Ren, L. Gao, B. Liu, S. Pei, H.-M. Cheng, *Nat. Mater.* **2011**, *10*, 424.
[15] C. Li, G. Shi, *Nanoscale* **2012**, *4*, 5549.
[16] V. Chabot, D. Higgins, A. Yu, X. Xiao, Z. Chen, J. Zhang, *Energy Environ. Sci.* **2014**, *7*, 1564.
[17] L. Qiu, J. Z. Liu, S. L. Y. Chang, Y. Wu, D. Li, *Nat. Commun.* **2012**, *3*, 1241.
[18] X. Cao, Y. Shi, W. Shi, G. Lu, X. Huang, Q. Yan, Q. Zhang, H. Zhang, *Small* **2011**, *7*, 3163.
[19] Y. Zhao, C. Hu, Y. Hu, H. Cheng, G. Shi, L. Qu, *Angew. Chem. Int. Ed.* **2012**, *51*, 11371.
[20] W. Lv, Y. Tao, W. Ni, Z. Zhou, F.-Y. Su, X.-C. Chen, F.-M. Jin, Q.-H. Yang, *J. Mater. Chem.* **2011**, *21*, 12352.
[21] H. Sun, Z. Xu, C. Gao, *Adv. Mater.* **2013**, *25*, 2554.
[22] Z. Xu, C. Gao, *Acc. Chem. Res.* **2014**, *47*, 1267.
[23] Y. Wu, N. Yi, L. Huang, T. Zhang, S. Fang, H. Chang, N. Li, J. Oh, J. A. Lee, M. Kozlov, A. C. Chipara, H. Terrones, P. Xiao, G. Long, Y. Huang, F. Zhang, L. Zhang, X. Lepró, C. Haines, M. D. Lima, N. P. Lopez, L. P. Rajukumar, A. L. Elias, S. Feng, S. J. Kim, N. T. Narayanan, P. M. Ajayan, M. Terrones, A. Aliev, P. Chu, Z. Zhang, R. H. Baughman, Y. Chen, *Nat. Commun.* **2015**, *6*, 6141.
[24] Y. Egami, T. Yamamoto, K. Suzuki, T. Yasuhara, E. Higuchi, H. Inoue, *J. Mater. Sci.* **2011**, *47*, 382.
[25] W. Li, T. Wu, W. Wang, P. Zhai, J. Guan, *J. Appl. Phys.* **2014**, *116*, 044110.
[26] G. Sun, B. Dong, M. Cao, B. Wei, C. Hu, *Chem. Mater.* **2011**, *23*, 1587.
[27] J. Liu, R. Che, H. Chen, F. Zhang, F. Xia, Q. Wu, M. Wang, *Small* **2012**, *8*, 1214.
[28] R. Che, L. M. Peng, X. F. Duan, Q. Chen, X. Liang, *Adv. Mater.* **2004**, *16*, 401.
[29] J. Liu, J. Xu, R. Che, H. Chen, Z. Liu, F. Xia, *J. Mater. Chem.* **2012**, *22*, 9277.
[30] C.-J. Li, B. Wang, J.-N. Wang, *J. Magn. Magn. Mater.* **2012**, *324*, 1305.
[31] Z. Chen, C. Xu, C. Ma, W. Ren, H. M. Cheng, *Adv. Mater.* **2013**, *25*, 1296.
[32] F. Moglie, D. Micheli, S. Laurenzi, M. Marchetti, V. M. Primiani, *Carbon* **2012**, *50*, 1972.
[33] R. Kumar, S. R. Dhakate, T. Gupta, P. Saini, B. P. Singh, R. B. Mathur, *J. Mater. Chem. A* **2013**, *1*, 5727.
[34] T. Zou, N. Zhao, C. Shi, J. Li, *Bull. Mater. Sci.* **2011**, *34*, 75.
[35] G. Wang, Z. Gao, S. Tang, C. Chen, F. Duan, S. Zhao, S. Lin, Y. Feng, L. Zhou, Y. Qin, *ACS Nano* **2012**, *6*, 11009.
[36] IEEE Std 521-2002 (Revision of IEEE Std 521-1984) **2003**, 0_1.
[37] Y. Yang, M. C. Gupta, K. L. Dudley, R. W. Lawrence, *Nano Lett.* **2005**, *5*, 2131.
[38] V. Weston, *IEEE Trans. Antenn. Propag.* **1963**, *11*, 578.
[39] Z. Fang, C. Li, J. Sun, H. Zhang, J. Zhang, *Carbon* **2007**, *45*, 2873.
[40] H. Zhang, J. Zhang, H. Zhang, *Comput. Mater. Sci.* **2007**, *38*, 857.
[41] W. L. Song, M. S. Cao, M. M. Lu, J. Yang, H. F. Ju, Z. L. Hou, J. Liu, J. Yuan, L. Z. Fan, *Nanotechnology* **2013**, *24*, 115708.
[42] N. Yousefi, X. Sun, X. Lin, X. Shen, J. Jia, B. Zhang, B. Tang, M. Chan, J. K. Kim, *Adv. Mater.* **2014**, *26*, 5480.